Full title: Mapping glioma heterogeneity using multiparametric ^{18}F-choline PET/MRI in childhood and teenage-young adults.

Short title: Cho PET/MRI in TYA gliomas.

Valentina Ferrazzoli[a], Ananth Shankar[b], Julia V. Cockle[b], Christine Tang[a], Ahmed Al-Khayfawee[a], Jamshed Bomanji[c], Francesco Fraioli[c] and Harpreet Hyare[d,e]

HH and FF share last author.

[a] *Department of Nuclear Medicine, University College London Hospitals NHS Foundation Trust, London UK*

[b] *Department of Paediatric & Adolescent Oncology, University College London Hospitals NHS Foundation Trust, London, UK.*

[c] *Institute of Nuclear Medicine, University College London, London, UK.*

[d] *Department of Imaging, University College London Hospital NHS Foundation Trust, London, UK.*

[e] *Department of Brain Repair and Rehabilitation, London, UK.*

Corresponding author: Dr Harpreet Hyare PhD

Department of Imaging

University College London Hospitals NHS Trust

235 Euston Road

London NW1 2BU UK

Telephone number: +44 20 3447 9070 / 9297

Email address: harpreet.hyare@nhs.net

Funding: This work was supported by the UCLH/UCL NIHR Biomedical Research Centre. FF received a grant support for tracer costing by the Rosetrees Trust charity foundation.

Conflicts of interest: There are no conflicts of interest.

Abstract

Objective: The heterogeneity of post-treatment imaging remains a significant challenge in children and teenagers/young adults (TYA) diagnosed with glioma. The aim of this study is to evaluate the utility of ^{18}F-choline PET/MRI in determining intratumoural heterogeneity in paediatric and TYA gliomas.

Methods: 26 patients (mean age 16 years, range 8–22 years) with suspected glioma disease progression were evaluated with ^{18}F-choline PET/MRI. Relative cerebral blood volume (rCBV), apparent diffusion coefficient (ADC) and maximum standardised uptake values (SUV_{max}) in enhancing (enh) and non-enhancing (ne) tumour volumes and normal-appearing white matter (wm) were calculated ($rCBV_{enh}$, $rCBV_{ne}$, $rCBV_{wm}$, ADC_{enh}, ADC_{ne}, ADC_{wm}, SUV_{enh}, SUV_{ne}, SUV_{wm}).

Results: Significantly higher SUV_{enh} and SUV_{ne} compared with SUV_{wm} were observed [SUV_{enh} 0.89 (0.23–1.90), SUV_{ne} 0.36 (0.16–0.78) versus SUV_{wm} 0.15 (0.04–1.19); P<0.001 and P=0.004, respectively]. Equivalent results were observed for ADV and rCBV (ADC_{enh}, ADC_{ne}: P<0.001 versus ADC_{wm}; $rCBV_{enh}$, $rCBV_{ne}$: P<0.001 versus $rCBV_{wm}$). The highest values for mean SUV_{max} [0.89 (0.23–1.90)] and mean rCBV [2.1 (0.74–5.08)] were in the enhancing component, while the highest values for ADC [1780 mm^2/s (863–2811)] were in the necrotic component.

Conclusion: ^{18}F-choline PET/MRI is able map imaging heterogeneity in paediatric and TYA gliomas, detecting post-treatment enhancing, non-enhancing, and necrotic tumour components equivalent to ADC and DSC-derived rCBV. This offers potential in the response assessment of diffuse non-enhancing gliomas and in selected cases such as posterior fossa tumours where quantitative MRI is technically difficult.

Keywords: ^{18}F-choline PET, magnetic resonance imaging, glioma

Introduction

Central nervous system (CNS) tumours remain the most common cause of cancer death in the US paediatric population and gliomas are the second leading cause of cancer mortality in adults under the age of 35 years [1,2]. In children and teenagers/young adults (TYA), astrocytoma represents the most frequent histology among CNS malignancies and high-grade gliomas cause the greatest proportion of deaths [1,3]. Despite new therapeutic strategies, including inhibiting angiogenesis and immunotherapy [4], progress has been limited by the inherent difficulties in assessing treatment response in clinical trials. The efficacy of traditional imaging response assessment utilising measurements of enhancing tumour on T1-weighted MRI [5] has been limited by the phenomena of *pseudoprogression*, whereby an increase in tumour volume, oedema and enhancement shortly after completion of treatment is often difficult to distinguish from tumour progression [6,7], and *pseudoresponse,* whereby a dramatic reduction in tumour enhancement following treatment with anti-angiogenic agents is thought to be due to vascular normalisation rather than a true anti-tumour effect [8,9]. Although the current most widely used response assessment criteria for high-grade gliomas, known as the RANO (Response Assessment in Neuro-Oncology) criteria, correct for a number of these complexities [10], there is still reliance on bidimensional measurements of contrast-enhancing tumour.

The role of positron emission tomography (PET) has recently been discussed by the RANO working group, with specific emphasis on PET with amino acid tracers as a functional imaging technique that might help in the evaluation of treatment response [2]. Nevertheless, routine clinical application has been delayed by several factors, including limited availability, legislation and high cost [11-13] and, apart from a small case series [14], this modality has not been widely investigated in paediatric and TYA patients. Among the non-amino acid tracers, ^{18}F-choline, a well-established tracer of phospholipid metabolism and cell membrane synthesis, is widely available at reasonable cost and shows excellent discrimination between tumour and normal tissue in the brain [15]. Limited series have investigated this tracer for assessment of treatment response in adult gliomas [16-18] but to our knowledge it has not been widely investigated in

paediatric/TYA gliomas and has not been used to map the heterogeneity of glioma imaging appearance. In this study we aim to quantify ^{18}F-choline uptake in different glioma tumour components in comparison with the more established quantitative measures of apparent diffusion coefficient (ADC) and dynamic susceptibility (DSC)-derived relative cerebral blood volume (rCBV) on a hybrid PET/MRI system. Our hypothesis is that choline is elevated in the enhancing component compared with other parts of the tumour.

Materials and methods

Patient population

26 consecutive children and TYA patients (mean age 14 years, range 6–21 years) with suspected clinical disease progression and referral for ^{18}F-choline PET/MRI between 2011 and 2017 were included, following departmental approval. Patient clinical details are shown in Table 1. Histological diagnoses included pilocytic astrocytoma (*n*=9), glioblastoma multiforme (*n*=6), anaplastic astrocytoma (*n*=4), and diffuse astrocytoma (*n*=2); histological diagnosis was not available in two patients. Timing of the first ^{18}F-choline PET/MRI in relation to the patient's surgery varied from 1 week to 550 weeks (Table 1). In four patients undergoing imaging surveillance, ^{18}F-choline PET/MRI was performed prior to surgery. Disease progression was confirmed by histological analysis (12 patients had surgical procedure/biopsy) or clinical–radiological evaluation at follow-up, where repeat MRI demonstrated an increase in volume of the tumour and/or increased enhancement. Patients were followed up for 2 years or until death.

^{18}F-choline PET/MRI protocol

All studies were performed on a 3T PET/MRI hybrid scanner (Siemens Healthineers, Erlangen, Germany). PET images were acquired 40 min after an intravenous injection of ^{18}F-fluoroethylcholine (4 MBq/kg). The duration of the scan was 10 min with one single bed acquired. Ultrashort echo sequences were acquired for MR-based attenuation correction [echo time (TE) 0.07 ms; repetition time (TR) 11.9 ms; flip angle 10°; slice thickness (st) 1.6 mm]. Using the attenuation-corrected PET images, standardised uptake value (SUV) images were calculated accounting for the time between injection and acquisition and the tracer half-life. PET data were acquired simultaneously with the MRI sequences under standard resting conditions.

The MRI protocol included an axial T2-weighted (w) inversion-recovery acquisition (TE/TR 397/5000, st 4 mm), an axial T2-w TSE sequence (TE/TR 300/4000, st 4 mm) and an axial T1-w 3D isovolumetric interpolated breath-hold sequence before and after gadolinium (0.2 ml/kg) injection (TE/TR 3.8/2000, voxel

size 1.1×1.1× 1.1 mm). Diffusion-weighted imaging (DWI) (TE/TR 100/8000, st 5 mm) was acquired using a single-shot echo-planar sequence in the axial plane with three b-values (0, 500 and 1000 s/mm^2). DSC perfusion-weighted imaging (PWI) was acquired after a preload dose administration of gadolinium-based contrast agent (GBCA) (0.005–0.1 mmol/kg) to partially correct for GBCA extravasation-induced T1 effects. DSC-PWI data (gradient-echo echo-planar imaging with TR/TE/flip angle 1500–2000 ms/20 ms/60°, FOV 24×24 cm, 5 mm section, no gap) were acquired during 3 min with the bolus injection occurring at the 1 min mark after the start of the DSC sequence.

Image analysis

Qualitative

Two neuroradiologists (HH, CT) assessed the conventional MRI scans using five VASARI criteria (https://wiki.cancerimagingarchive.net/display/Public/VASARI+Research+Project): (i) f1 tumour location, (ii) f2 side of tumour epicentre, (iii) f4 enhancement quality (no enhancement 0; minimal/mild 1, marked/avid 2), (iv) f5 proportion enhancing of whole tumour (none 0, <5% 1, 6%–33% 2, 34%–66% 3, 67%–95% 4, >95% 5) and (v) tumour markup (maximal perpendicular diameters.)

Quantitative

A radiologist with 3 years' experience in neuroimaging, blinded to the ^{18}F-choline PET images, manually drew the whole tumour volume (V_t), the volume of enhancing tumour (V_{enh}), the volume of non-enhancing tumour (V_{ne}) and a 2×2 cm region of interest (ROI) in the normal-appearing white matter on the T1-w post-contrast images, using T2W and FLAIR images as references on a dedicated platform (ITK-SNAP; v3.6.0) (Fig. 1).

Perfusion maps were obtained using a commercially available post-processing software (IBNeuro v.2.0; Imaging Biometrics) with a semi-automated arterial input function method. We normalised all rCBV maps with 3×3 voxel ROIs within the contralateral normal-appearing white matter. The raw perfusion frames

were averaged and then registered to the T1-w post-contrast MRI with advanced neuroimaging tools (ANTs; v2.2.0) [19]. The ADC and SUV maps were also independently rigidly registered to the T1-w image. Using the registered images, the mean ADC, mean rCBV and SUV_{max} in V_{enh}, V_{ne} and normal-appearing white matter (wm) were calculated (ADC_{enh}, ADC_{ne}, ADC_{wm}, $rCBV_{enh}$, $rCBV_{ne}$, $rCBV_{wm}$, SUV_{enh}, SUV_{ne}, SUV_{wm}).

Statistical analysis

Statistical analysis was performed using MedCalc, v.18.5 (MedCalc Software, Ostend, Belgium). Pearson correlation coefficient for non-categorical variables was used to establish the concordance between rCBV, ADC and SUV_{max}. Independent Student's t tests were applied to compare rCBV, ADC and SUV_{max} values within the different tumour components. A two-tailed *P* value less than 0.05 was considered significant.

Results

Qualitative analysis

The results of the qualitative MRI analysis are provided in Table 2. Most of the tumours were located in the basal ganglia (*n*=6), followed by the thalamus (*n*=4). The enhancement quality was predominantly marked/avid (*n*=12) with the most common proportion enhancing being 34–66% (*n*=6). Nine tumours demonstrated minimal/mild enhancement with the most common proportion enhancing <5% (*n*=6). Three tumours did not demonstrate enhancement and one patient did not receive contrast. The average tumour mark-up was 39.2±27.0 × 28.5±19.7 mm.

Figure 2 is a representative example of the hybrid ^{18}F-choline PET/MRI obtained in a 16-year-old patient diagnosed with diffuse astrocytoma demonstrating non-enhancing tumour on conventional MRI with foci of ^{18}F-choline uptake and increased perfusion seen in the right basal ganglia on the SUV and rCBV maps, respectively.

Quantitative tumour component analysis

Significantly higher mean SUV_{max} in the enhancing and non-enhancing tumour components compared with normal-appearing white matter was observed [0.89 (0.23–1.90) and 0.36 (0.16–0.78) versus 0.15 (0.04–1.19); *P*<0.001 and *P*=0.004, respectively] and the mean SUV_{max} in the enhancing component was significantly higher than that in the non-enhancing component (Table 3 and Fig. 3). Significantly higher ADC and rCBV in enhancing and non-enhancing tumour components were also demonstrated compared with normal white matter. The highest values for mean SUV_{max} [0.89 (0.23–1.90)] and mean rCBV [2.1 (0.74–5.08)] were in the enhancing component, while the highest values for ADC [1780 mm^2/s (863–2811)] were in the necrotic component (Fig. 3). There was no correlation between SUV_{max}, rCBV and ADC (ADV versus SUV, *r*=0.298, rCBV versus SUV, *r*=0.143).

Discussion

To our knowledge, this is the first study to have demonstrated that quantitative ^{18}F-choline PET/MRI can map glioma imaging heterogeneity in paediatric and TYA gliomas. We have shown that quantitative ^{18}F-choline PET/MRI can discriminate enhancing and non-enhancing tumour from normal brain parenchyma, equivalent to ADC and rCBV. In particular, increased ^{18}F-choline SUV was seen in non-enhancing tumour compared with normal-appearing white matter and offers potential for the evaluation of treatment response in diffuse non-enhancing gliomas. In this population, a multimodal quantitative ^{18}F-choline PET/MRI approach can be used to effectively evaluate post-treatment tumour in selected cases where MRI is equivocal for tumour progression and quantitative MRI is technically difficult.

PET imaging is increasingly being used in the still-challenging field of brain tumour response assessment. The 2016 recommendations of the RANO working group and the European Association for Neuro-Oncology suggested the use of amino acid PET with this aim, endorsing the role of multimodality imaging [2]. Although a recent meta-analysis has shown that the diagnostic accuracy is not as high as amino acid tracers [20], ^{18}F-fluorocholine, a marker of enhanced cell proliferation, is widely available, is less expensive than other tracers and has favourable pharmacokinetic features [21]. Several previous studies have evaluated the role of ^{18}F-choline PET/CT in low- and high-grade gliomas [22-25] but few studies have examined intra-tumoural heterogeneity. In a recent series of four low-grade glioma patients, foci of increased ^{18}F-choline SUV defined the anaplastic tumour component [26].

To our knowledge, this is the first study to quantitatively evaluate glioma heterogeneity with ^{18}F-choline PET/MRI on a hybrid MRI system which allows optimal spatial and temporal realignment of the metabolic and morphological images with more reliable SUV values within tumour volumes; moreover, the rCBV and ADC maps were co-registered with morphological sequences in order to be consistent with ROI placement for the tumour component analysis.

SUV_{max} was able to distinguish both enhancing and non-enhancing tumour components from normal-appearing white matter, mirroring the ADC and rCBV findings and reflecting enhanced cell proliferation in tumours [24]. ADC has been shown to correlate inversely with tumour cell density, with lower ADC values in high-grade tumours and high ADC values in peritumoural oedema [27], while rCBV reliably correlates with tumour grade, vascularity and focal anaplastic transformation [28]. We also found no significant correlation between SUV_{max}, ADC and rCBV in the different tumour components, suggesting that each interrogates and reflects different properties of the tumour and that they should be viewed as complementary.

Other PET tracers are available and, considering their different mechanisms of uptake and specificity, the choice of tracer may vary depending on the tumour type. Amino acid tracers have shown higher diagnostic accuracy than MRI in the evaluation of treatment-related changes and treatment response [2]: *O*-2-^{18}F-fluoroethyl-L-tyrosine (^{18}F-FET) uptake is highly increased in grade III/IV gliomas and its dynamic evaluation can help in grading [29], while 3,4-dihydroxy-6-^{18}F-fluoro-L-phenylalanine (^{18}F-FDOPA) has demonstrated high potential in defining tumour grade and outcome when combined with DWI and PWI in a paediatric population [14,30]. A recent report described a combined ^{18}F-choline PET/MRI approach in the evaluation of CNS lymphoma post-treatment [31]; a similar multimodal approach in gliomas offers the potential for improved response assessment in paediatric and TYA gliomas.

Our study has some limitations. First, we considered only SUV_{max}, not taking into account other metabolic parameters such as tissue-to-background ratio (TBR) and metabolic tumour volume. However, SUV_{max} is the most commonly used parameter and it allows easier comparison between studies. Furthermore, while the TBR parameter is important for other tracers showing a variable degree of background uptake, that is, ^{18}F-DOPA and ^{18}FET, ^{18}F-choline shows limited if any uptake in the grey and white matter, which means that the background contributes very little for brain tumours.

We did not investigate the correlation between imaging features and molecular profile, which influences perfusion values and the metabolic uptake of gliomas in the adult population [32,33], due to incomplete molecular genetic data. However, considering the spectrum of molecular alterations in childhood and TYA brain tumours, this will be a future field of investigation.

Conclusion

^{18}F-choline PET is able map imaging heterogeneity in paediatric and TYA gliomas, detecting post-treatment enhancing, non-enhancing and necrotic tumour components equivalent to ADC and DSC-derived rCBV. This offers potential in the response assessment of diffuse non-enhancing gliomas and in selected cases where quantitative MRI is technically difficult, such as in posterior fossa tumours. A quantitative multimodal ^{18}F-choline PET/MRI approach can better define the different components of residual tumour, improving the assessment of treatment response in this patient group.

Consent to participate

This study was performed on anonymised clinical PET/MRI scans performed as part of the patients' normal clinical pathway for which consent was not required.

Consent for publication

This study was performed on anonymised clinical PET/MRI scans performed as part of the patients' normal clinical pathway for which consent was not required.

Availability of data and material

All data are available on direct request to the corresponding author.

Code availability

Not applicable.

References

1. Ostrom QT, Gittleman H, Fulop J, et al. CBTRUS statistical report: primary brain and central nervous system tumors diagnosed in the United States in 2008-2012. *Neuro Oncol*. 2015; 4:iv1-iv62.

2. Albert NL, Weller M, Suchorska B, et al. Response Assessment in Neuro-Oncology working group and European Association for Neuro-Oncology recommendations for the clinical use of PET imaging in gliomas. *Neuro Oncol.* 2016; 18:1199-1208.

3. Georgakis MK, Panagopoulou P, Papathoma P, et al. Central nervous system tumours among adolescents and young adults (15-39 years) in Southern and Eastern Europe: Registration improvements reveal higher incidence rates compared to the US . *Eur J Canc.* 2017; 86: 46-58.

4. Hottinger AF, Aissa AB, Espeli V, et al. Phase I study of sorafenib combined with radiation therapy and temozolomide as first-line treatment of high-grade glioma. *Br J Cancer*. 2014; 110:2655-2661.

5. Macdonald DR, Cascino TL, Schold SC, et al. Response criteria for phase II studies of supratentorial malignant glioma. *J Clin Oncol*. 1990; 8: 1277-1280.

6. Young RJ, Gupta A, Shah AD, et al. Potential utility of conventional MRI signs in diagnosing pseudoprogression in glioblastoma. *Neurology.* 2011; 76:1918-1924.

7. Verma N, Cowperthwaite MC, Burnett MG, Markey MK. Differentiating tumor recurrence from treatment necrosis: a review of neuro-oncologic imaging strategies. *Neuro Oncol*. 2013; 15:515-534.

8. Norden AD, Drappatz J, Wen PY. Novel anti-angiogenic therapies for malignant gliomas. *Lancet Neurol*. 2008; 7:1152-1160.

9. Narayana A, Kelly P, Golfinos J et al. Antiangiogenic therapy using bevacizumab in recurrent high-grade glioma: impact on local control and patient survival. *J Neurosurg*. 2009; 110:173-180.

10. Wen PY, Macdonald DR, Reardon DA, et al. Updated Response Assessment Criteria for High-Grade Gliomas: Response Assessment in Neuro-Oncology Working Group. *J Clin Oncol*. 2009; 28:1963-1972.

11. Stauss J Franzius C, Pfluger T, et al. Guidelines for 18F-FDG PET and PET-CT imaging in paediatric oncology. *Eur J Nucl Med Mol Imaging*. 2008; 35: 1581-8.

12. Pauleit D, Stoffels G, Bachofner A, et al (2009). Comparison of (18)F-FET and (18)F-FDG PET in brain tumors. *Nucl Med Biol*. 2009; 36:779–78.

13. Heiss WD, Raab P, Lanfermann H. (2011). Multimodality assessment of brain tumors and tumor recurrence. *J Nucl Med. 2011;* 52:1585–1600.

14. Morana G, Piccardo A, Tortora D, et al. Grading and outcome prediction of pediatric diffuse astrocytic tumors with diffusion and arterial spin labeling perfusion MRI in comparison with 18F-DOPA PET. *Eur J Nucl Med Mol Imaging*. 2017; 44: 2084-2093.

15. Mertens K, Slaets D, Lambert B, Acou M, De Vos F, Goethals I. PET with (18)F-labelled choline-based tracers for tumour imaging: a review of the literature. *Eur J Nucl Med Mol Imaging*. 2010; 37:2188-2193.

16. Li FM, Nie Q, Wang RM, et al. 11C-CHO PET in optimization of target volume delineation and treatment regimens in postoperative radiotherapy for brain gliomas. *Nucl Med Biol*. 2012; 39:437-442.

17. Li W, Ma L, Wang X, et al. (11)C-choline PET/CT tumor recurrence detection and survival prediction in post-treatment patients with high-grade gliomas. *Tumour Biol*. 2014; 35: 12353-12360.

18. Bolcaen J, Acou M, Boterberg T et al. 18F-FCho PET and MRI for the prediction of response in glioblastoma patients according to the RANO criteria. *Nucl Med Commun*. 2017; 242-249.

19. Avants BB, Tustison NJ, Song G, Cook PA, Klein A, Gee JC. A reproducible evaluation of ANTs similarity metric performance in brain image registration. *NeuroImage*. 2011; 54: 2033–2044.

20. Zwart PL, van Dijken BRJ, Holtman, GA et al. Diagnostic accuracy of PET tracers for the differentiation of tumour progression from treatment-related changes in high grade glioma: a systematic review and metaanalysis. *J of Nuc Med.* 2020; 61(4): 498-504.

21. Mertens K, Bolcaen J, Ham H, et al. The optimal timing for imaging brain tumours and other brain lesions with 18F-labelled fluoromethylcholine: a dynamic positron emission tomography study. *Nucl Med Commun*. 2012; 33: 954-959.

22. Kwee SA, Ko JP, Jiang CS, et al. Solitary Brain Lesions Enhancing at MR Imaging: Evaluation with Fluorine 18-Fluorocholine PET. *Radiology*. 2007; 557-565.

23. Mertens K, Ham H, Deblaere K, et al. Distribution patterns of 18F-labelled fluoromethylcholine in normal structures and tumors of the head: a PET/MRI evaluation. *Clin Nucl Med*. 2012; 37: e196-e203.

24. Fraioli F, ShankarA, Hargrave D, et al. 18F-Fluoroethylcholine (18F-Cho) PET/MRI FunctionalParameters in Pediatric Astrocytic Brain Tumors. *Clin Nucl Med* . 2015; 40: e40-e45.

25. Gomez-Rio M, Testart Dardel N, Santiago Chinchilla A, et al. 18F-Fluorocholine PET/CT as a complementary tool in the follow-up of low-grade glioma: diagnostic accuracy and clinical utility. *Eur J Nucl Med Mol Imaging*. 2015; 42: 886-895.

26. Vicente AMG, Garcia JMC, Menendez CL et al. Low-grade versus high grade glioma…That is the question. 18F-Fluorocholine PET in the detection of anaplastic focus. *Clin Nucl Med*. 2020; 45:394-397.

27. Hayashida Y, Hirai T, Morishita S, et al. Diffusion-weighted imaging of metastatic brain tumours: comparison with histologic type and tumor cellularity. *AJNR*. 2006; 27: 1419-1425.

28. Lacerda S, Law M. Magnetic resonance perfusion and permeability imaging in brain tumors. *Neuroimaging Clin North Am. 2009;* 19: 527-557.

29. Pöpperl G, Kreth FW, Mehrkens JH, et al. FET PET for the evaluation of untreated gliomas: correlation of FET uptake and uptake kinetics with tumour grading. *Eur J Nucl Med Mol Imaging*. 2007; 34:1933-1942.

30. Morana G, Piccardo A, Milanaccio C, et al. Value of 18F-3,4-dihydroxyphenylalanine PET/MR image fusion in pediatric supratentorial infiltrative astrocytomas: a prospective pilot study . *J Nucl Med*. 2014; 55: 718-723.

31. Kowa J-Y, Millard T, Goldman A, et al. Are treatment response assessment maps (TRAMs) and 18F choline positron emission tomography the future of central nervous system lymphoma imaging? British Journal of Haematology. 2021; 195, e97-e119.

32. Leu K, Ott GA, Lai A, et al. Perfusion and diffusion MRI signatures in histologic and genetic subtypes of WHO grade II-II diffuse gliomas. *J Neurooncol*. 2017; 134: 177-188.

33. Verger A, Metellus P, Sala Q, et al. IDH mutation is paradoxically associated with higher 18F-FDOPA PET uptake in diffuse grade II and grade III gliomas. *Eur J Nucl Med Mol Imaging*. 2017; 44: 1036-1311.

Tables and Figures:

Figure 1: MRI demonstrating regions of interest

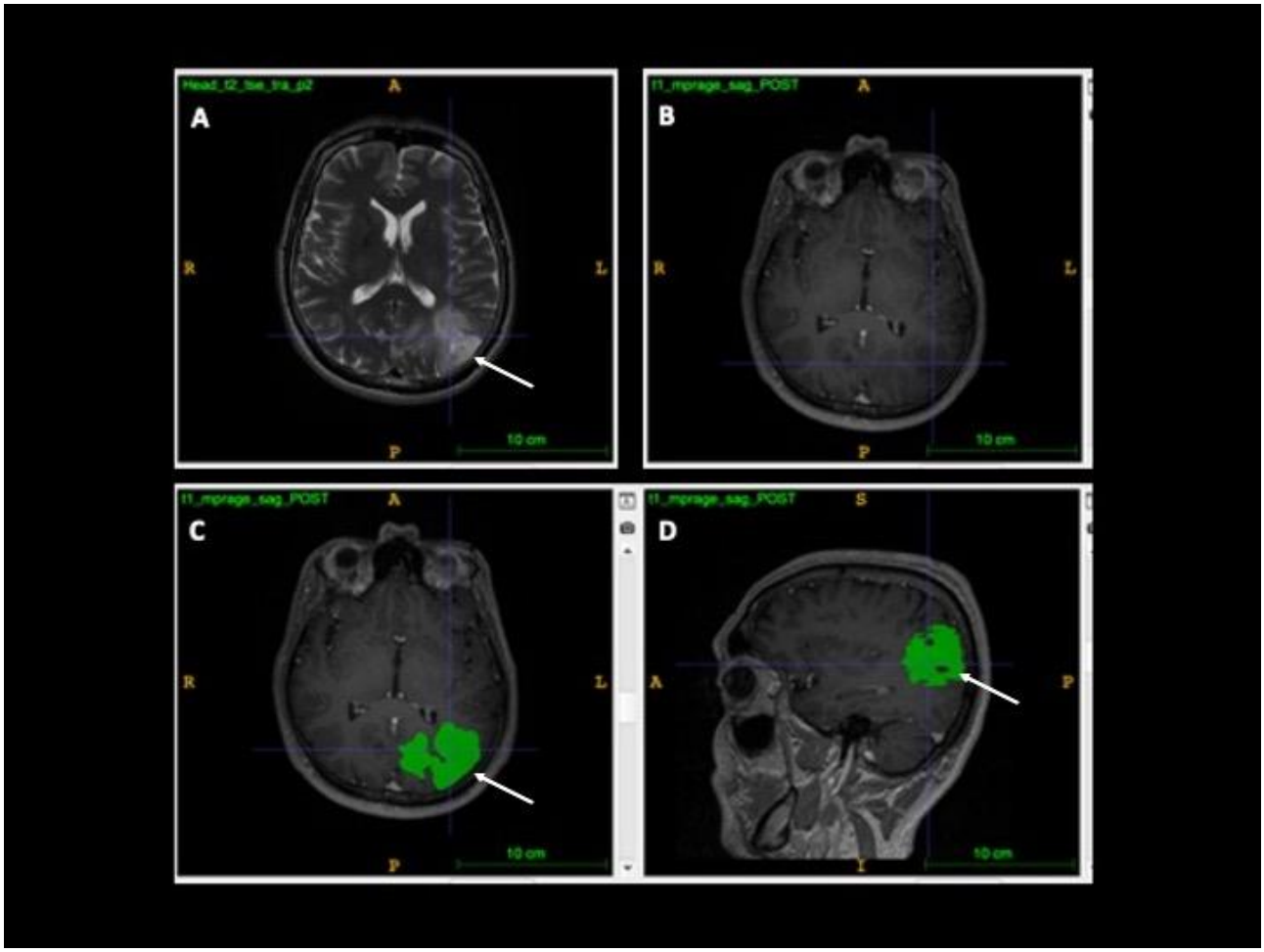

Fig. 1: MRI demonstrating regions of interest in a 14-year-old male with pathologically proven diffuse astrocytoma. (A) T2-w axial image demonstrates a large area of T2-w signal abnormality in the left occipital lobe. (B) There is no associated pathological enhancement. (C) and (D) T1-w post-contrast images demonstrate the non-enhancing region of interest (green) in (C) axial and (D) para-sagittal planes.

Figure 2: ^{18}F-choline PET/MRI.

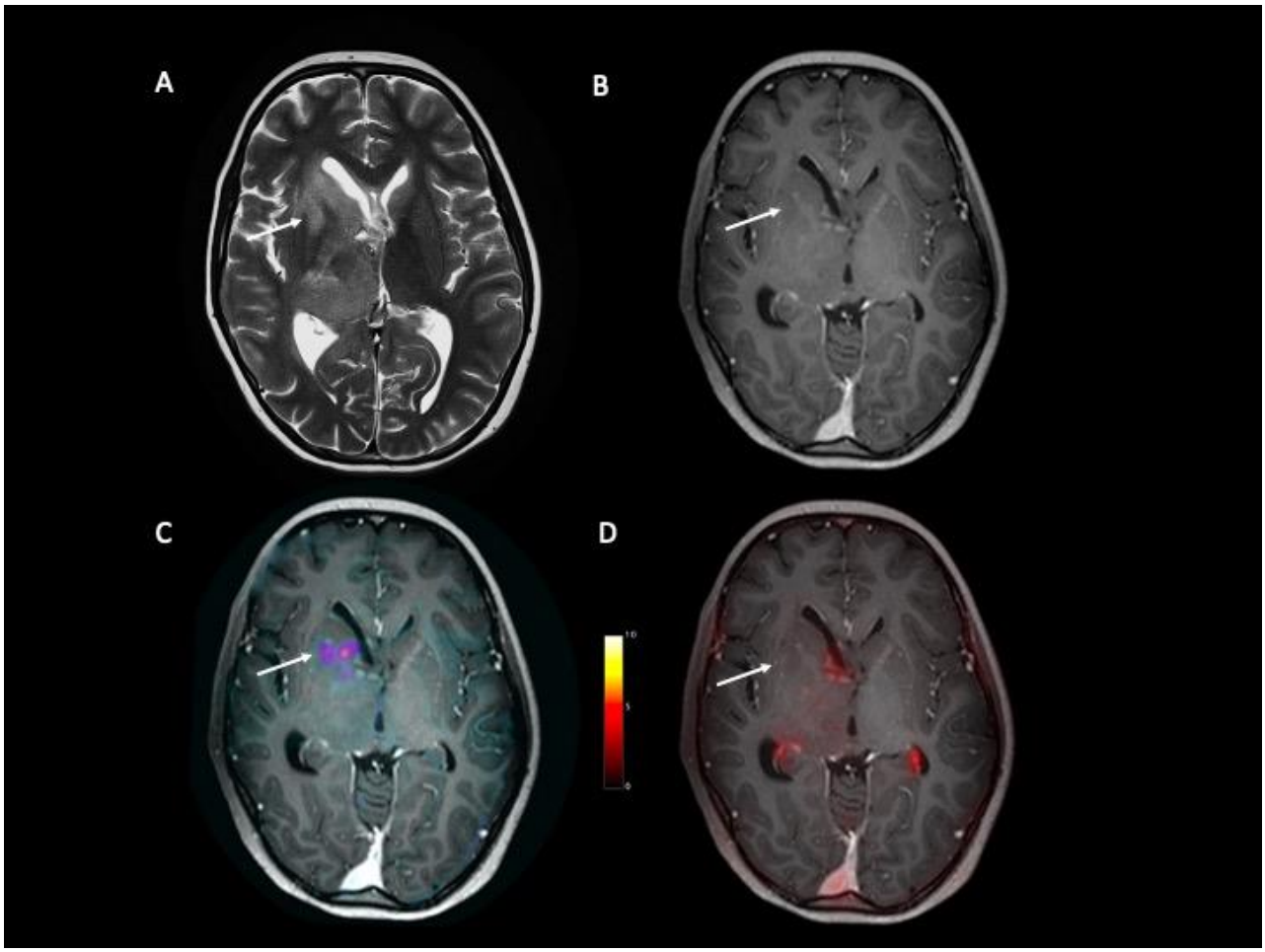

Figure 2: ^{18}F-choline PET/MRI in a 16-year-old male with pathologically proven GBM. Four months after the end of treatment, a large area of abnormal signal in the right basal ganglia and thalamus is seen on the axial T2-w image (A), with an area of faint enhancement in the right head of caudate on the T1-w post-contrast image (B). The ^{18}F-choline PET image fused with the post-contrast T1-w image (C) shows increased SUV in the anterior non-enhancing component of the residual tumour and the rCBV map fused with the T1-w post-contrast image (D) also demonstrates significant increased uptake in the same region.

Figure 3: Plotted SUV_{max} values, ADC and rCBV in different tumour components.

A

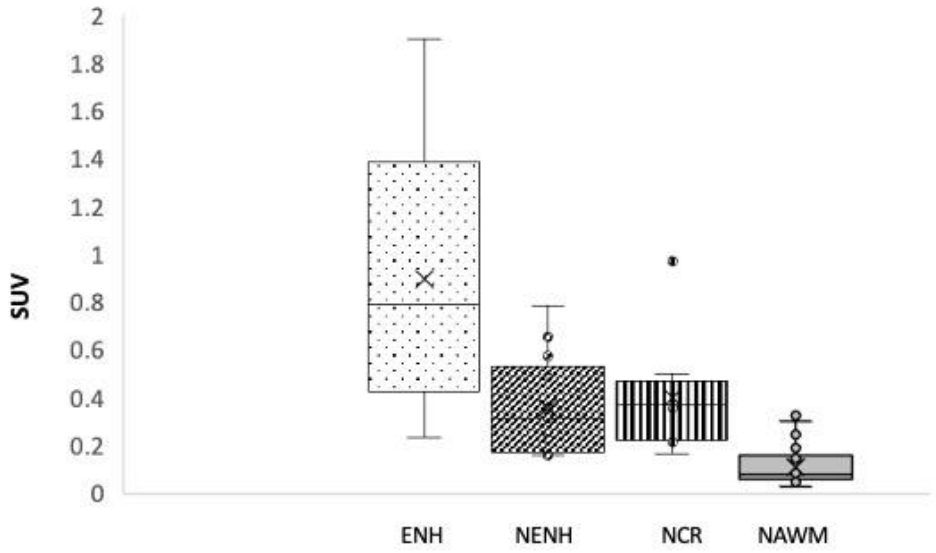

B

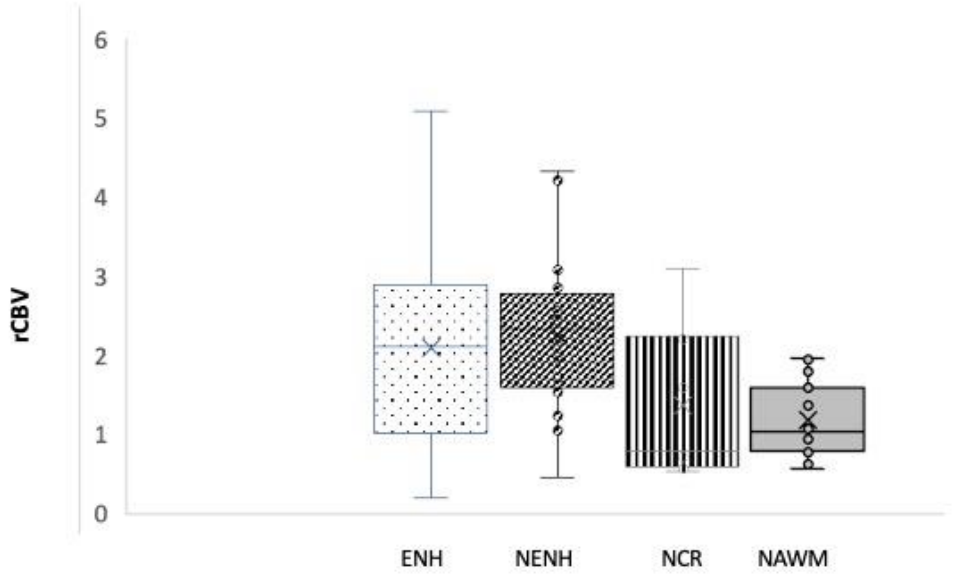

C

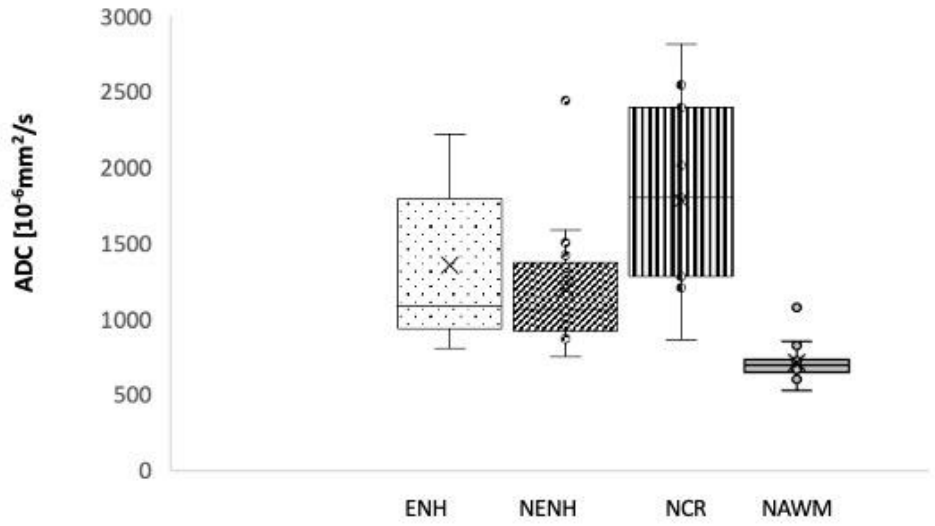

Figure 3: Plotted SUV_{max} values, ADC and rCBV in different tumour components, illustrating the SUV_{max}, ADC and rCBV in the enhancing, non-enhancing and necrotic tumour components compared with normal-appearing white matter. Abbreviations: ADC, apparent diffusion coefficient; ENH, enhancing component; NAWM, normal-appearing white matter; NECR, necrosis; NENH, non-enhancing component; rCBV, relative cerebral blood volume; SUV, standardised uptake value.

Patient	Age (y)	Sex	Tumour location	Surgery	Radiotherapy	Chemotherapy	Grade	Histology	Molecular pathology	Treatment at disease progression	OS (m)
1	6	F	Medulla	–	–	–	LGG	PA	–	–	–
2	7	F	Basal ganglia	B *	Nil	Vincristine, carboplatin	HGG	GBM	GFAP +ve IDH WT	RT, TMZ	7
3	8	M	Medulla	SR	54 Gy in 30♯	TMZ	HGG	–	–	–	–
4	8	F	Basal ganglia	–	–	–	HGG	–	–	–	–
5	10	F	Frontal	SR	54 Gy in 30♯	TMZ	HGG	AA	–	Sirolimus	20
6	11	F	Pineal	SR	54 Gy in 30♯	TMZ	HGG	GBM	GFAP +ve IDH WT BRAF M –ve	Bevacizumab	18
7	12	M	Frontal	B	Nil	Vinblastine	LGG	PA	–	N/A	A
8	12	F	Thalamus	B	54 Gy in 30♯	Nil	LGG	PA	–	N/A	A
9	13	F	Medulla	B	Nil	Vinblastine	LGG	PA	–	RT, irinotecan, bevacizumab	17
10	13	F	Basal ganglia	B	54 Gy in 30♯	TMZ	HGG	AA	–	Lomustine	24
11	14	F	Basal ganglia	SR	54 Gy in 30♯	TMZ	HGG	GBM	MGMT –ve GFAP +ve IDH WT	RT, afatinib, lomustine	29
12	14	F	Basal ganglia	B	54 Gy in 30♯	TMZ	HGG	AA	–	PCV	12
13	15	M	Cerebellum	SR	Nil	Nil	LGG	PA	–	Surgery	A
14	16	M	Thalamus	SR	54 Gy in 30♯	TMZ Bevacizumab	HGG	GBM	GFAP +ve IDH WT	RT	8
15	16	M	Basal ganglia	B	50.1 Gy in 30♯	TMZ	LGG	DA	–	TMZ	A
16	16	F	Frontal	B	54 Gy in 30♯ PBT	TMZ	LGG	DA	IDH mutant MGMT –ve H3F3A –ve BRAF M –ve	N/A	A
17	17	M	Fronto-parietal	B	59.4 Gy in 33♯	TMZ	HGG	AA	–	Lomustine	10
18	17	F	Pons	B	54 Gy in 30♯	TMZ	HGG	GBM	–	N/A	A
19	17	M	Thalamus	B	Nil	Nil	LGG	PA	IDH WT BRAF M +ve	Surveillance/ considering surgery	A
20	17	M	Thalamus	B	54 Gy in 30♯	Nil	LGG	PA	GFAP +ve IDH WT	n/a	A
21	18	M	Pons	B	54 Gy in 30♯	TMZ, PCV	HGG	DMG	H3K27M +ve	RT, TMZ	14
22	18	M	Fronto-parietal	B	54 Gy in 30♯	TMZ	HGG	GC	–	RT, TMZ	91
23	19	M	Hypothalamus	SR	54 Gy in 30♯	Nil	LGG	PA	GFAP +ve	Surgery, vincristine Carboplatin	A
24	19	F	Cerebellum	TR	Nil	Nil	LGG	PA	KIAA1549– BRAF +ve	RT, TMZ	A
25	20	F	Temporal	SR	60 Gy in 30♯	TMZ	HGG	GBM	IDH mutant	N/A	–
26	20	F	Frontal	B	Nil	Vincristine, carboplatin, cisplatin, cyclophosphamide	LGG	Ganglioglioma	–	N/A	A

Table 1: Patient clinical history

Abbreviations: A, alive; AA, anaplastic astrocytoma; B, biopsy; BRAF M, BRAF mutation; DA, diffuse astrocytoma; DMG, diffuse midline glioma; GBM, glioblastoma multiforme; GC, gliomatosis cerebri; GFAP, glial fibrillary acidic protein; HGG, high-grade glioma; IDH WT, isocitrate dehydrogenase wild-type; LGG, low-grade glioma; m, months (to the nearest month); MGMT, O6-methylguanine-DNA methyltransferase; N/A, non-applicable; NF1, neurofibromatosis type 1; OS, overall survival; PA, pilocytic astrocytoma; PBT, proton beam therapy; PCV, procarbazine, lomustine (CCNU), vincristine; RT, radiotherapy; SR, subtotal resection; TMZ, temozolomide; TR, total resection; y, years.
* Biopsy done at time of disease progression

Table 1: Patient clinical history. Illustration of the tumour histology, grade and molecular genetics, treatment regimen, treatment at disease progression and overall survival

Table 2: Tumour MRI characteristics

Patient	F1 Tumour location	F2 Side of tumour	F4 Enhancement quality	F5 Proportion enhancing (%)	Tumour markup: longest axis (mm)	Tumour markup: longest perpendicular axis (mm)
1	Medulla	Midline	Minimal/mild	6–33	22	19.3
2	Basal ganglia	Right	Marked/avid	34–66	74.1	38.7
3	Medulla	Midline	Minimal/mild	>95	10.3	10
4	Basal ganglia	Left	Marked/avid	34–66	54.9	32.6
5	Frontal	Left	Minimal/mild	<5	54.7	48.0
6	Pineal	Midline	Minimal/mild	<5	19.1	8.9
7	Frontal	Right	Minimal/mild	<5	95.6	52.4
8	Thalamus	Left	Marked/avid	>95	28.5	25.2
9	Medulla	Midline	No contrast	N/A	12.2	7.8
10	Basal ganglia	Left	Mild	6–33	25	39
11	Basal ganglia	Left	Minimal/mild	<5	45.2	41.5
12	Basal ganglia	Left	Minimal/mild	<5	26.4	20.2
13	Cerebellum	Midline	Marked/avid	67–95	26	8
14	Thalamus	Right	None	N/A	55	24.9
15	Basal ganglia	Right	Minimal/mild	6–33	17.2	14.8
16	Frontal	Right	None	N/A	21.9	33.1
17	Fronto-parietal	Right	Minimal/mild	<5	95.6	52.4
18	Pons	Midline	None	N/A	28.8	28.4
19	Thalamus	Left	Marked/avid	34–66	38.9	27.3
20	Thalamus	Left	Marked/avid	34–66	33.5	23.6
21	Pons	Midline	Marked/avid	6–33	35.2	33.6
22	Fronto-parietal	Right	Marked/avid	34–66	101	93.5
23	Hypothalamus	Right	Marked/avid	34–66	51.4	36.6
24	Cerebellum	Midline	Marked/avid	6–33	8.3	1.4
25	Temporal	Right	Marked/avid	67–95	32.8	14.8
26	Frontal	Left	Marked/avid	>95	7.3	5.2

Table 2: Qualitative tumour MRI characteristics. Illustration of MRI VASARI criteria: f1 Tumour location, f2 Side of lesion, F3 enhancement quality, f4 proportion enhancing, and tumour markup: longest diameter and longest perpendicular diameter (mm). N/A, non-applicable.

Table 3: Tumour component analysis

ROI	Enh[a]	Ne[b]	Nec	WM[c]	*P* value a vs c	*P* value b vs c	*P* value a vs b
Mean SUV_{max} (range)	0.89 (0.23–1.90)	0.36 (0.16–0.78)	0.4 (0.16–0.97)	0.15 (0.04–1.19)	<0.001*	0.004*	<0.001*
Mean ADC (mm^2/s) (range)	1356 (805–2218)	1198 (750–2439)	1780 (863–2811)	710 (524–1078)	<0.001*	<0.001*	0.158
Mean rCBV (range)	2.1 (0.74–5.08)	2.27 (1.08–4.34)	1.38 (0.54–3.09)	1.17 (0.57–1.96)	<0.001*	<0.001*	0.304

Abbreviations: ADC, apparent diffusion coefficient; Enh, enhancing tumour; Ne, non-enhancing tumour; Nec, necrosis; rCBV, relative cerebral blood volume; ROI, region of interest; SUV_{max}, maximum standardised uptake value; WM, white matter. **P* value statistically significant.

Table 3: Tumour component analysis. Demonstrates the mean $SUV_{max,}$ mean ADC (mm^2/s) and mean rCBV in the enhancing, non-enhancing and necrotic components of the tumour compared with normal-appearing white matter.